Journal of Membrane Science and Research 7 (2021) 295-304

Journal of Membrane Science & Research

journal homepage: www.msrjournal.com

Research Paper

Morphology and Topography Studies of Composite Membranes Developed from Chitosan/Phthaloyl Chitosan Consisting Multi-Walled Carbon Nanotube/Montmorillonite as Filler

Arif Priyangga [1], Zuhriah Mumtazah [1], Hazlina Junoh [2], Juhana Jaafar [2], Lukman Atmaja [1,*]

[1] *Department of Chemistry, Institut Teknologi Sepuluh Nopember, ITS Sukolilo, Surabaya 60111, Indonesia*
[2] *Advanced Membrane Technology (AMTEC) Research Centre, Universiti Teknologi Malaysia, 81310 UTM Johor Bahru, Johor, Malaysia*

Article info

Received 2020-03-22
Revised 2020-10-17
Accepted 2020-11-06
Available online 2020-11-06

Keywords

Chitosan
Carbon nanotube
Morphology
Topography
Direct methanol fuel cell

Highlights

- Cs/PhCs/MWCNT/MMT have been fabricated using solvent evaporation method for DMFC.
- The addition of MWCNT/MMT filler diminishes methanol permeability of the membranes.
- The MWCNT/MMT filler also increases the membrane selectivity.
- The addition of 7.5wt.% MWCNT/MMT into matrix achieves the maximum power density.
- The excessive amount of filler causes the agglomeration in the membrane surface.

Graphical abstract

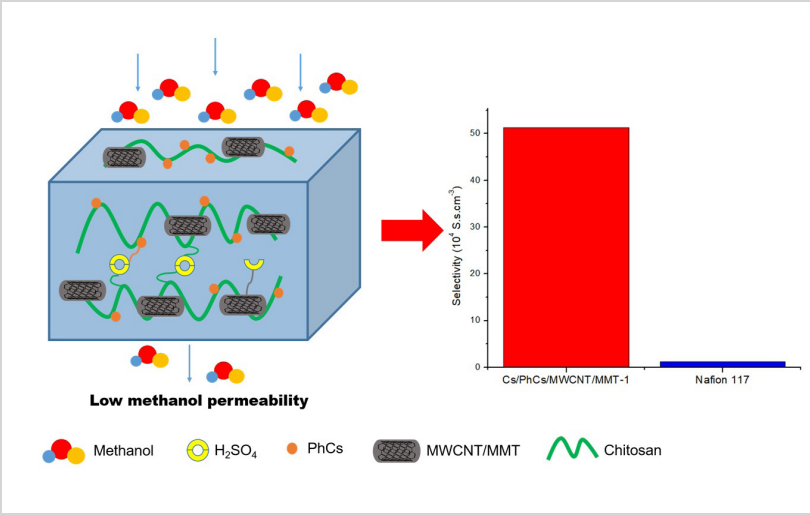

Abstract

This work discusses the synthesis and characterizations of the newly developed composite membranes based on chitosan/phthaloyl chitosan (Cs/PhCs) as a matrix with various compositions of multi-walled carbon nanotube/montmorillonite (MWCNT/MMT) filler. The Cs/PhCs/MWCNT/MMT composite membranes are synthesized via the solvent evaporation method and were investigated by Fourier Transform Infrared (FTIR), Atomic Force Microscopy (AFM), Scanning Electron Microscopy (SEM), Electrochemical Impedance Spectroscopy (EIS), and DMFC single cell test. The FTIR characterization result showed that all membranes have origin peaks at 3433, 2943, and 1525 cm^{-1} contributed to vibrations of O-H, C-H, and N-H group, respectively. Meanwhile, the composite membranes with 7.5 and 8 wt.% filler have characteristic peaks of vibration Si-O-Si, Si-OH, and Si-O at 1209, 886, and 591 cm^{-1} respectively. Cross-sectional micrographs of SEM and AFM revealed that the composite membrane with 7.5 wt.% filler had moderate surface roughness than the other as-fabricated membranes. As a result, this nanocomposite membrane can be an alternative polyelectrolyte membrane for DMFC applications. The resulting Cs/PhCs/MWCNT/MMT-1 composite membrane has the selectivity up to 5.13×10^5 S.s.cm^{-3} with the DMFC performance at 23.60 mW cm^{-2}.

1. Introduction

Fossil fuel is the main global energy source and it is projected to increase by 56% in 2040 due to various factors such as rapid population growth, industrial development, and urbanization. Combustion of fossil fuels in the energy sectors which mainly produces CO_2 could contribute to climate change and global warming [1,2]. One of the promising alternatives for clean and efficient energy source is the fuel cell. Fuel cells are preferred as a better energy source as a result of their low sulfur oxide and nitrogen emission compared to fossil fuel [3]. It can tackle the energy crisis in the future. Technically, a fuel cell is a tool that changes chemical substance to direct electrical current as long as oxidant and fuel are constantly supplied. Chemical energy for fuel cells such as methanol and ethanol is considered environmentally friendly substances [4]. There are several kinds of fuel cells including direct methanol fuel cell (DMFC) that has numerous advantages such as high productivity, easy to operate, and no pollution released [5].

* Corresponding author:E-mail address: lukman_at@chem.its.ac.id (L. Atmaja)

DOI: 10.22079/JMSR.2020.123415.1357

There are three main components in DMFC such as anode, cathode, and electrolyte. The important material used in DMFC that acts as both electrolyte and separator is the polymer electrolyte membrane (PEM). It is used as a proton pathway that connects anode to cathode [6,7]. The most common PEM that is employed as an electrolyte in the fuel cell is Nafion. Nafion has been commercially operated as a PEM due to good chemical stability, good mechanical, and high conductivity. The presence of sulfonic acid groups introduces the proton transportation process [8]. However, the performance of Nafion tends to decrease when it is operated at above 80 °C [9]. Some essential properties that must be possessed by a composite membrane in order to be considered as PEM are high conductivity and power density, low methanol permeability, and persist at a high operating temperature [10-12]. Nowadays, the specification of the PEM which can be applied for transportation is larger than 100 °C. It aims to reduce the contamination of anode catalysts as a result of carbon monoxide (CO) [13]. These problems have boosted the interest of the researchers in the development of a new alternative membrane with excellent performances.

In recent years, chitosan (Cs) has been developed as an attractive material and it is used as a base biopolymer for the fuel cell membrane. Chitosan can be obtained from shrimp, crab, or lobster shells through the deacetylation process with the degree of deacetylation above 50% [14]. Typically, chitosan is highly recommended because of its non-toxicity, biodegradable, good film-forming, low cost, environmentally friendly, abundance, and chemically easy to modify [15,16]. The ability to withstand the high-temperature operation is a key factor for PEM to be considered as a good performance. However, poor mechanical strength, low thermal degradation and instability under high temperatures have limited the usage of pristine chitosan [10,11]. Besides that, the rigidity and crystallinity of pristine chitosan are high. These features have made chitosan only dissolve in a specific solvent. The weakness of chitosan can be solved by incorporating chitosan with other materials. Phthalic anhydride is highly recommended to incorporate with chitosan because it can increase the performance of chitosan, especially to improve the proton conductivity and thermal stability [10]. Proton conductivity is one of the most important properties in terms of proton transfer in the polyelectrolyte membrane. Generally, there are two categories of proton transfer mechanisms in the PEM: Grotthus (proton hopping) and vehicular mechanism (diffusion) which involve ion exchange capacity (IEC) and the water uptake of the membrane, respectively [11].

Inorganic material also can be used as a material to reinforce chitosan for composite membranes. Many inorganic materials have been used and studied as filler for chitosan. The addition of inorganic materials as filler played an important role to form microstructure and build the stability between the hydrophilic-hydrophobic groups in the membrane structure [10]. Furthermore, the filler can also increase the thermal and mechanical stability of membranes [12]. Many studies have reported the performance of silica as filler in different membranes. Silica is favorable to increase the proton conductivity of membranes due to its characteristic to absorb water even at high temperatures [17]. Zhao et al. [18] applied Cs/PHMSS-ATMP as the PEM in DMFC which showed a high conductivity of 9.4×10^{-2} S cm^{-1} when it occurred at 110 °C. Yin et al. [19] fabricated a blended membrane of Cs/Ti-Si functionalized carboxyl and amine groups. This inorganic material enhances the proton conductivity value up to 0.0408 $S.cm^{-1}$ with the highest selectivity of 4.85×10^4 $S.s.cm^{-3}$ (3 times compared to the chitosan membrane). Thermal stability also showed that the temperature degradation of the hybrid membrane is at 210 °C. It can be inferred that the hybrid membrane can operate above 100 °C in the fuel cell. Silica-rich material like MMT also can be used as filler for the chitosan membrane which can improve the thermal degradation of the pure chitosan membrane. Purwanto et al. [11] observed chitosan/montmorillonite-GPTMS which has a degradation temperature of 514.5 °C compared to the pure chitosan membrane that has 498.5 °C.

In recent years, carbon nanotube (CNT) has gradually taken the attention of researchers to research and develop it due to the tremendous mechanical and physical strength, low density, and high modulus young, as well as thermal stability. Those properties attract many researchers to develop new materials in various applications such as electronic devices, sensors, catalysis, energy storage, and superconductor [20-23]. CNT is the one-dimensional carbon material that is made and rolled up from one or more graphene sheets. The synthesis processes of CNT involve various techniques such as the arc evaporation method, chemical vapor deposition, and laser ablation [24]. One twisted graphene sheet is well-known as the single-walled carbon nanotube (SWCNT), more than one twisted graphene sheet also well-known as the multi-walled carbon nanotube (MWCNT) [24]. In the carbon nanotube surface, π-π electron interaction makes the surfaces of CNT have high energy and stability. This characteristic makes CNT insoluble and hard to be homogeneously dispersed in the polymer matrix [25]. The easiest way to make CNT soluble in the polymer matrix is by applying functionalization. One of the types of functionalization is using strong acids so that it can introduce other functional groups on CNT. Furthermore, functionalized CNT can be incorporated with silica-rich material like MMT to further enhance the properties of both CNT and MMT [24]. As we know, incorporation between MWCNT and silica-rich material (MMT) has not been reported yet. This study aims to synthesize and characterize the newly developed Cs/PhCs/MWCNT/MMT composite membranes. The morphology and topography of the membranes before and after adding MWCNT/MMT filler was investigated using SEM and AFM, respectively. Hopefully, this composite membrane could be a reference to fabricate the polyelectrolyte membrane for a fuel cell application.

2. Experimental

2. 1. Materials

Dry shrimp shell residue of *Litopenaeus vannamei* was applied as a chitosan resource. Montmorillonite (MMT) powder and Multi-Walled Carbon Nanotube (MWCNT) were acquired from Sigma-Aldrich. Ethanol (C_2H_5OH), nitric acid (HNO_3), methanol (CH_3OH), acetic acid (CH_3COOH), N, N-dimethylformamide (C_3H_7NO), sodium hydroxide (NaOH), phthalic anhydride ($C_8H_4O_3$), and ammonia solution (NH_3) were purchased from Merck. Nitrogen gas (N_2), sulfuric acid (H_2SO_4), diethyl ether ($C_4H_{10}O$), and hydrochloric acid (HCl) were obtained from the Smart Lab Indonesia.

2.2. Chitosan extraction

Chitosan was isolated originating at dry shrimp shell (*Litopenaeus vannamei*) agreeing to the prior study [11]. Initially, the dry shrimp shell was mashed to become dry shrimp powder. The shrimp's powder was then added into 3.5 wt.% NaOH solution at 65 °C for 2 h. The combination was separated and the residue was washed until neutral. The residue was dried at 105 °C for 6 h. Then, the dried powder was demineralized using 1 M HCl solution with a ratio of 1:15 (w/v) at 65 °C for 30 min, rinsed until neutral, and dried at 105 °C for 6 h. This dried powder is known as chitin. Then, chitin was reacted over the deacetylation process by employing 50 wt.% NaOH solution at 120 °C for 4 h. The combination was separated, washed, and dried. The final dried powder is known as chitosan.

2.3. Modification chitosan with phthalic anhydride

The modified chitosan with phthalic anhydride was prepared corresponding to the process described by Muthumeenal et al. [10]. Initially, 64.5 g phthalic anhydride was reacted with 23.7 g chitosan powder in 100 mL of DMF and nitrogen atmosphere at 130 °C for 5 h. Ice water was then added into the resulting combination to precipitate and obtain phthaloyl chitosan (PhCs). Moreover, it was separated and further refined using ethanol and diethyl ether.

2.4. Synthesis of MWCNT/MMT filler

Initially, 1 g MWCNT was dispersed into the mixture of strong acid HNO_3/H_2SO_4 with a ratio of 3:1 (v/v) at 100 °C for 6 h. Furthermore, it was cooled at 25 °C. Then, 1000 mL of deionized water was added to the mixture. The black solid MWCNT was separated and neutralized repeatedly until pH = 7. The black residue was then redispersed in 12 M HCl 100 mL for 12 h at 100 °C. HCl was used as an acid post-treatment to form a new carboxylic functional group at the MWCNT structure. The suspension was separated and dried at 100 °C for 10 h to obtain oxidized MWCNT (o-MWCNT). MWCNT/MMT was synthesized through the sol-gel method. The black solid o-MWCNT was ultrasonically dispersed into a combination of ethanol, NH_4OH, and deionized water with a ratio of 20:1:10 (v/v/v) for 30 min. Then, 1 g MMT was added into the suspension and stirred at 25 °C for 12 h. The subsequent suspension was separated and the residue was ultrasonicated in DMF for 15 min. Finally, it was separated and dehydrated under a vacuum at 70 °C for 12 h.

2.5. Cs/PhCs/MWCNT/MMT membranes fabrication

In this work, the Cs/PhCs membrane was prepared using 2 g chitosan dissolved in 2 wt.% acetic acid solution (80 mL). It was then stirred and ultrasonicated for 30 min. In another beaker, 0.05 g solid PhCs were initially dissolved into 10 mL DMF and stirred for 30 min. Cs and PhCs solution were mixed and stirred to obtain the homogeneous Cs/PhCs gel solution. The combination was then poured into acrylic casting and dried under room temperature for about 2 weeks. The resulting membrane was soaked in 1 M NaOH solution for 15 min then neutralized using deionized water. For the

proton pathway, the membrane was finally soaked in 1 M H_2SO_4 solution for 12 h, re-neutralized using deionized water, and dried at 25 °C.

The Cs/PhCs/MWCNT/MMT composite membranes were fabricated using the solvent evaporation process follow the same procedure. Initially, MWCNT/MMT filler was suspended in 2 wt.% acetic acid for 30 min and poured into the as-prepared Cs/PhCs solution. The combination was stirred until obtaining the black solution. Then, the solution was cast in acrylic casting and dehydrated under room temperature for 2 weeks. The composite membranes were initially soaked in 1 M NaOH solution for 15 min and then neutralized. Finally, it was soaked in 1 M H_2SO_4 solution for 12 h, re-neutralized, and dried at room temperature. The resulting composite membrane was known as Cs/PhCs/MWCNT/MMT membrane. The compositions of the composite membranes are listed in Table 1.

Table 1
Membranes composition.

Membrane	Cs (wt.%)	PhCs (wt.%)	MWCNT/MMT (wt.%)
Cs/PhCs	90	10.0	0
Cs/PhCs/MWCNT/MMT-1	90	2.5	7.5
Cs/PhCs/MWCNT/MMT-2	90	2.0	8.0

2.6. Membrane characterization

In this research, FTIR is used to investigate the interaction of functional groups for all samples. All samples were crushed and mixed with 0.6-1.0 g of refining grade KBr to form a homogeneous powder. Then, it was pressed using a hydraulic press to form a pellet. The pellet was scanned using the wavenumber of 4000-400 cm^{-1}.

The physicochemical properties of membranes were examined. The methanol permeability test was conducted using two compartments in which compartment A and B containing water and methanol, respectively. The results of the experiment were calculated using Eq. (1):

$$P = \left(\frac{\Delta C_B}{\Delta t}\right) \times \left(\frac{d \times V_A}{A \times C_B}\right) \quad (1)$$

$\Delta C_B/\Delta t$ is the difference of methanol concentration in compartment B as time function (mol L^{-1} s^{-1}), P is the methanol permeability ($cm^2.s^{-1}$), A is the surface area (cm^2), d is the membrane's thickness (cm), V_A is the water volume at compartment A (cm^3), and C_B is the methanol concentration in the compartment B (mol L^{-1}). The conductivity was determined by EIS (Autolab PGSTAT204 system from Metrohm). All impedance measurements were conducted at 100% relative humidity (RH) and room temperature. The proton conductivity must follow the Eq. (2):

$$\sigma = \frac{L}{R \times A} \quad (2)$$

which σ is the proton conductivity (S cm^{-1}), R is the membrane resistance (Ω), L and A are the thickness (cm) and surface area (cm^2). Selectivity was calculated from the ratio between σ (conductivity) and P (methanol permeability). The higher selectivity is more favorable for fuel cell application. Before the DMFC test, the MEA was prepared using the hot press technique (120 °C, 2 MPa) for 3 min. The anode and cathode contained Pt-Ru/C and Pt/C, respectively. The anode was fuelled with methanol (5 M) and the cathode was fueled with oxygen using the flow rate of 1 mL min^{-1} and 50 mL min^{-1}, respectively. Water uptake calculation must follow Eq. (3):

$$WU\ (\%) = \frac{W_{wet} - W_{dry}}{W_{dry}} \times 100\% \quad (3)$$

where W_{dry} and W_{wet} are the membrane weight before and after soaking in water, respectively. To evaluate water uptake of the membrane, initially, the membrane was dehydrated at 50 °C for 24 h and then weighed. It was soaked in water for 24 h and gradually dried with a tissue and weighed again. The IEC was measured by the titration method. Initially, the membrane was dehydrated at 50 °C for 24 h and weighed. It was immersed in a 1 M NaCl solution 50 mL. Then, the solution was titrated using 0.01 M NaOH solution and phenolphthalein was added into the solution. IEC was calculated using Eq. (4):

$$IEC\ (meq.g^{-1}) = \frac{V_{NaOH} \times M_{NaOH}}{W_d} \quad (4)$$

V_{NaOH} is the volume of NaOH used for titration (mL), M_{NaOH} is the molality of NaOH, and W_d is the weight of the dried membrane (g).

The morphology of the membranes was analyzed by SEM for the cross-section and surface area. Moreover, the topography of the membranes was observed using AFM to evaluate the membrane's surface roughness. The membranes were cut within the size of 1 cm × 1 cm, placed into the sample holder and then scanned at the nanometer scale.

3. Result and discussion

3.1. FTIR of chitin and chitosan

FTIR analysis was conducted to confirm the synthesis of chitin or chitosan qualitatively. FTIR showed the specific bands of chitin and chitosan in which the peaks of chitin appeared at a wavenumber of 3447, 1665, and 2891 cm^{-1} which represent the hydroxyl, carbonyl, and methyl group respectively. Also, the peaks at 3266 and 3103 cm^{-1} indicated amide I. Glucopyranose ring (C-O-C) showed the stretching vibration at the wavenumber of 1034 cm^{-1}. Stretching vibration of C-N and C-O was showed at 1379 and 1157 cm^{-1} respectively [11]. The bands of chitosan were most likely chitin because chitosan was derived from chitin only as there were some shifts that occurred at the specific wavenumber such as hydroxyl groups (O-H) being shifted to a smaller wavenumber at 3433 cm^{-1} with the wider band. It was caused by the decrement of amide I that initially overlapping with O-H groups [26]. Furthermore, the decrement of intensity bands from carbonyl (1653 cm^{-1}) and amide II (1587 cm^{-1}) in chitosan revealed that the deacetylation process was successfully done [27]. It was also indicated that chitin was partially deacetylated into chitosan. The degree of deacetylation is an important parameter in chitosan. The bigger the degree of deacetylation, the easier for chitosan to incorporate with another material [26]. The IR spectra of chitin and chitosan are showed in Figure 1.

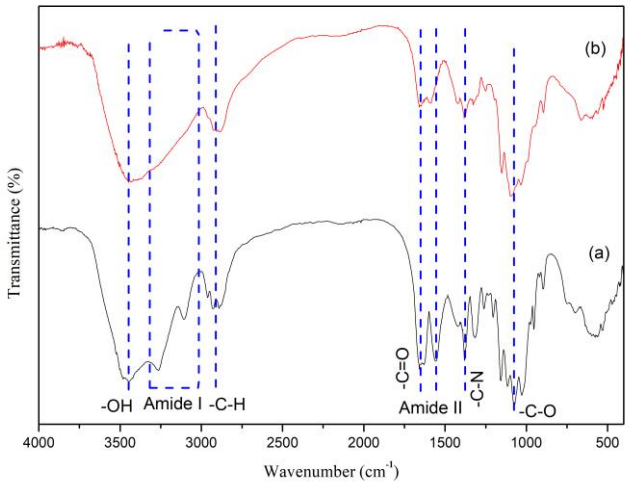

Fig. 1. IR spectra of (a) chitin, and (b) chitosan samples.

3.2. FTIR analysis of phthaloyl chitosan

Modification of Cs with phthalic anhydride was also conducted with FTIR to know the alteration of functional groups. The characteristic bands of PhCs appeared at a wavenumber of 3267 and 3107 cm^{-1} which indicated =C-H group while C=C aromatic rings were detected at 723 cm^{-1}. These bands were obtained from the benzene structure of phthalic anhydride [10]. Mostly, the specific peaks of Cs appeared again at PhCs bands such as O-H (3449), C-H (2992), C-N (1390), and C-O (1070 cm^{-1}). Carbonyl groups of PhCs have a

sharper band and shifted to a bigger wavenumber when it is compared to pristine Cs. The pristine Cs still has the carbonyl group band due to the partial deacetylation process. The partial deacetylation process makes the amide group from chitin still emerge in pristine Cs [10]. It was shifted from 1653 to 1712 cm^{-1} caused by two new carbonyl groups from phthalic anhydride that attached to the main structure of Cs. In addition, the C-N band of PhCs still exists and sharper than Cs due to the substitution of other functional groups to hydrogen molecules of Cs [28]. Muthumeenal et al. [10] reported the synthetic route of PhCs and showed the phthalic group still attached to $–NH_2$ group of Cs structure as shown in Figure 2. From these investigations, it can be concluded that new peaks from PhCs showed phthalic groups that have been substituted into Cs structure. The FTIR spectra of PhCs are shown in Figure 3.

3.3. FTIR analysis of filler MWCNT/MMT

MWCNT before and after modification with MMT were investigated by FTIR analysis. MWCNT before and after functionalization were also investigated. As shown in Figure 4, FTIR analysis revealed the alteration of MWCNT after functionalized. It revealed pure MWCNT and o-MWCNT still have two characteristic peaks that showed C-H stretching and C=C bending at wavenumber 2922 and 1535 cm^{-1}, respectively [29]. After oxidized, there are new characteristic bands that showed C=O and C–O stretching at 1736 and 1099 cm^{-1}, respectively. Stretching –OH group also appeared at 3414 cm^{-1} [21]. From these results, we can conclude that MWCNT was successfully oxidized using a mixed strong acid and did not affect the main structure of MWCNT.

Figure 5 shows the FTIR result of MWCNT/MMT filler. It showed the characteristic band for pure MWCNT still exists at 2924 cm^{-1} which is C-H stretching band. Also, it was confirmed by the C=C band at 1539 cm^{-1}. Furthermore, the band of stretching O-H appears at a wavenumber of 3423 cm^{-1}. The typical bands of MMT in filler that appear at 1055 and 799 cm^{-1} showed Si–O and –SiOH group, respectively [30]. C–O group band overlapped with the Si–O–Si group from MMT at 1055 cm^{-1}. It revealed which MMT has perfectly been modified by MWCNT. The addition of Si–O–Si group into MWCNT/MMT filler leads to the disappearance of the C=O group in MWCNT/MMT which substitutes the carboxylic group of oxidized MWCNT [24].

The possible modification process of MMT/MWCNT nanoparticles is shown in Figure 6. The CNT structure was attached to the MMT structure using both the MMT and MWCNT hydrophilic functional groups.

3.4. FTIR analysis of Cs/PhCs/MWCNT/MMT composite membranes

The resulting composite membranes were characterized using FTIR to know the chemical interaction of the membrane. It can be clearly shown in Figure 7 that Cs/PhCs membrane has characteristic bands of chitosan at 3445, 2934, 1532, and 1638 cm^{-1} with O-H, C-H, amide I, and amide II respectively. The resulting Cs/PhCs/MWCNT/MMT composite membranes also show the bands of chitosan at 3433, 2943, 1525, and 1630 cm^{-1}. But, the composite membranes possess the new bands of Si–O–Si, –SiOH, and Si–O groups that indicate the present of MWCNT/MMT filler at the wavenumber of 1209, 886, and 591 cm^{-1} whereby the Cs/PhCs membrane did not have these bands [24]. The shifting band of 1267 to 1209 cm^{-1}, 896 to 886 cm^{-1}, and a new band of 591 cm^{-1} has verified the existence of new groups in the membrane structure due to the addition of nanoparticle filler [23]. The bands of 1267 and 896 cm^{-1} typically come from the PhCs molecule. Besides that, Cs bands are dominantly existed due to the amount of Cs is more than PhCs or MWCNT/MMT. In this case, the composite membranes were successfully fabricated with good compatibility among matrix and nanoparticle filler.

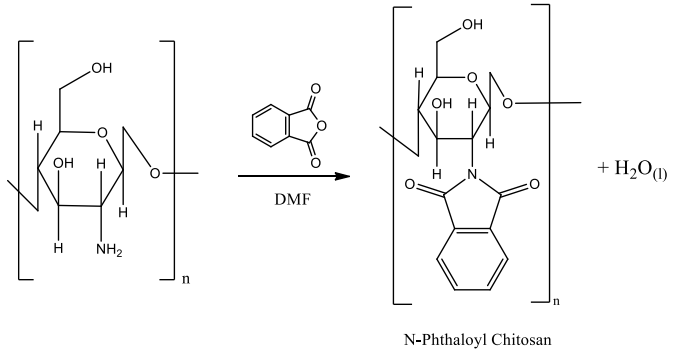

Fig. 2. The synthetic route of phthaloyl chitosan.

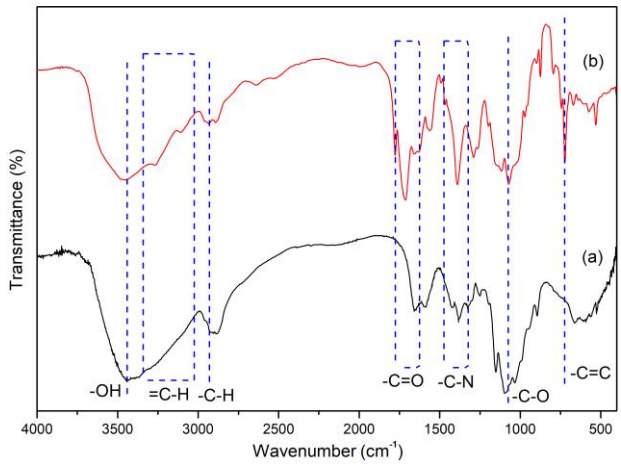

Fig. 3. IR spectra of (a) Cs, and (b) PhCs samples.

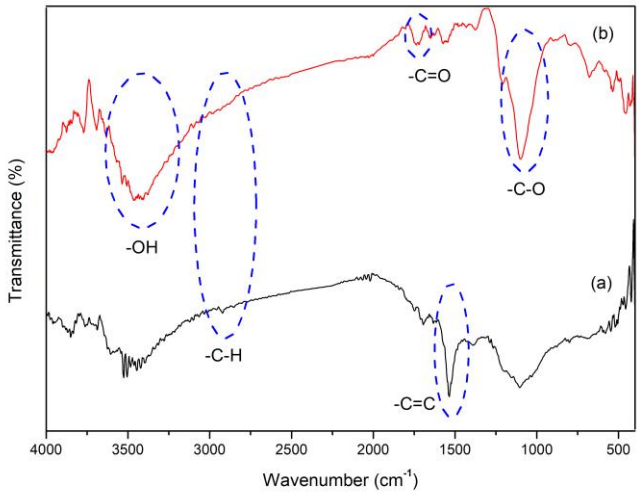

Fig. 4. IR spectra of (a) pristine MWCNT, and (b) oxidized MWCNT.

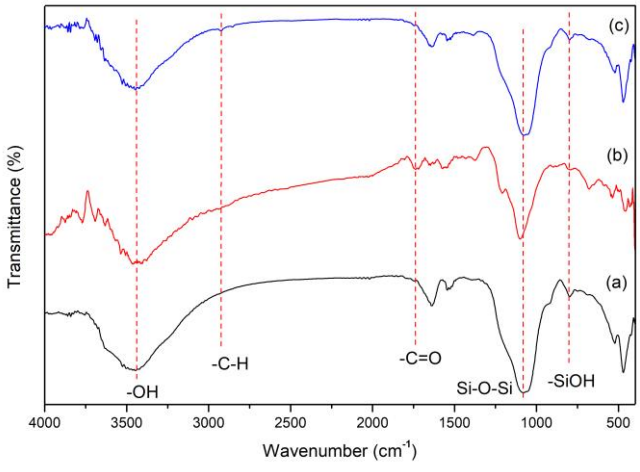

Fig. 5. FTIR spectra of (a) MMT, (b) oxidized MWCNT, and (c) MWCNT/MMT filler.

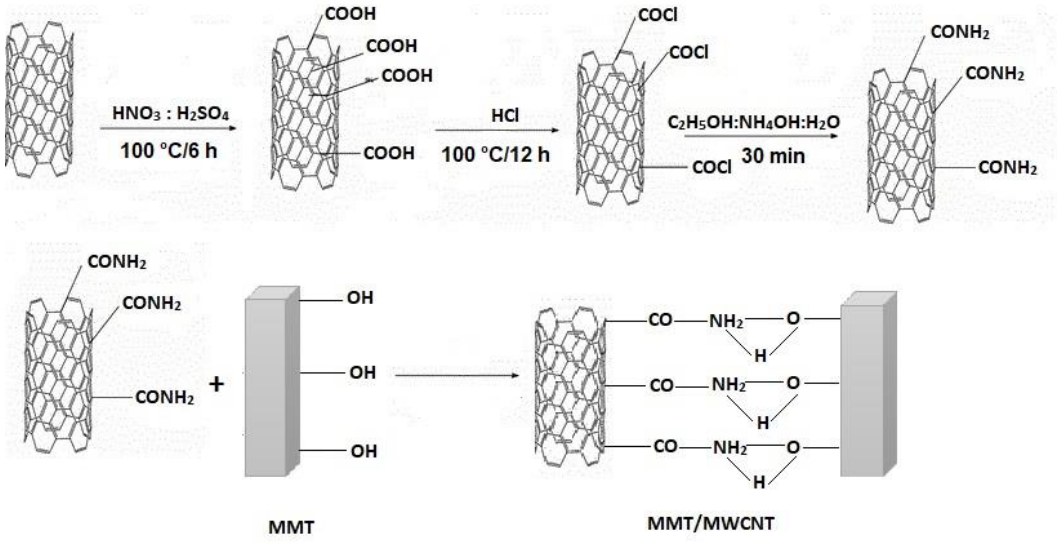

Fig. 6. Modification process of MMT/MWCNT nanoparticles.

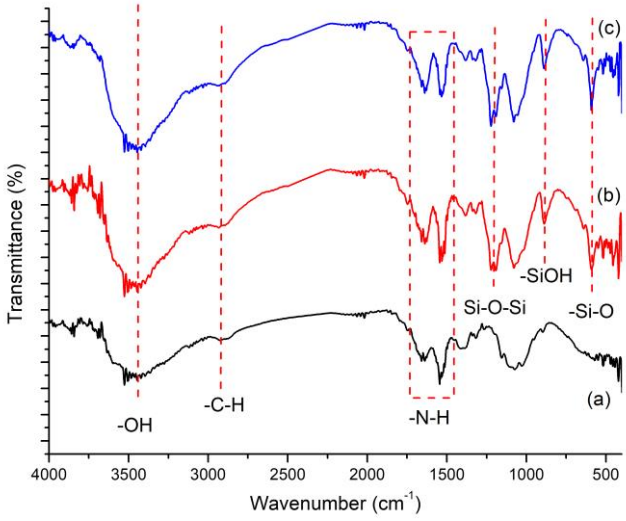

Fig. 7. IR spectra of membranes (a) Cs/PhCs, (b) Cs/PhCs/MWCNT/MMT-1, (c) Cs/PhCs/MWCNT/MMT-2.

3.5. Proton conductivity

Since conductivity takes a key role to measure the magnitude of the membrane power density, it is highly recommended to determine the membrane conductivity which could determine the effect of filler on the membrane performance [10,24]. In this work, a membrane incorporated with PhCs filler had a lower conductivity than the membrane incorporated with both the PhCs and MWCNT/MMT fillers. It showed that the proton conductivity of the Cs/PhCs membrane was at 2.44 mS cm^{-1}. The Cs/PhCs/MWCNT/MMT-1 membrane can reach proton conductivity up to 3.95 mS cm^{-1}. This phenomenon could be due to the role of functional groups attached to the membrane structure. The functional groups involved in the membrane structure comprised hydroxy, $-NH_3^+$, and Si-O groups. Mostly, these hydrophilic functional groups were obtained from MMT and Cs [11,31]. A higher density of functional groups is favorable in a typical membrane for a fuel cell. It can reduce ionic interaction in the proton-conducting network and increase the motion of protons [10,32]. The abundance of hydroxyl groups in MMT supports the membrane's structure to be able to provide an extra conduction site for proton transfer, hence increases the proton conductivity [11,31]. Since the two general principle mechanisms explain the proton transfer in the polymeric membranes such as "Grotthuss mechanism" or "proton hopping" and "Vehicular mechanism", it revealed the type of mechanism that could happen in the membrane's structure [33]. In this work, the Cs matrix and MMT facilitate an endless hydrophilic cluster that permits the protons to be transferred by "Vehicle mechanism". Moreover, for the electrostatic interaction between the Cs and MWCNT/MMT that contained many hydroxyl and $-NH_3^+$ groups, the proton was transported via the Grotthuss mechanism [11,31]. Consequently, this work suggests both the Vehicular and proton hopping mechanisms are involved in the proton conductivity of membranes. According to Peng et al. [22], MWCNT facilitates a high electrical conductivity for polymer-matrix materials. On the other hand, the o-MWCNT has a low electrical conductivity which is favorable and useful for PEM. The low electrical conductivity properties of o-MWCNT are in agreement with the conductivity of the membrane-based CNT that provides the proton pathway through the MWCNT's structure. These properties allow protons to travel in the membrane structure [8]. This characteristic could improve the resulting composite membrane performance. It shows in this work that Cs/PhCs/MWCNT/MMT-1 membrane had the highest proton conductivity among the other as-prepared membranes. However, the proton conductivity of 8 wt.% MWCNT/MMT filler was lower than 7.5 wt.% of the MWCNT/MMT filler. The large aggregation of MMT in the membrane structure could disrupt the proton conductivity [34]. The proton conductivity of membranes is listed in Table 2.

3.6. Methanol permeability

Since commercial membranes for fuel cell, Nafion consume enormous methanol of fuel in DMFC, it is important to seek an alternative membrane which has low methanol permeability [35]. Low methanol permeability plays a crucial role in DMFC as it provides a high-efficiency methanol usage and can reduce fuel loss. Nafion 117 is a commercial membrane that has a high-level methanol permeability of 2.50×10^{-6} $cm^2.s^{-1}$ [11]. The methanol permeability is shown in Table 2. The addition of MWCNT/MMT filler contributed to the reduction of the methanol permeability. Based on the table, it is clearly displayed that the lowest methanol permeability is Cs/PhCs/MWCNT/MMT-1. This membrane can only reach its permeability up to 7.71×10^{-9} $cm^2.s^{-1}$. Furthermore, the methanol permeability of Cs/PhCs/MWCNT/MMT-2 is still lower than Nafion 117. This indicates that the MWCNT/MMT filler is capable of decreasing the methanol permeability of the resulting composite membrane due to the characteristic of MMT and MWCNT structures that have a high width and nanostructure in nature. These structures have led to creating lengthier diffusion pathways for methanol to penetrate the membrane and reducing the resulting membrane pores to avoid excessive loss of methanol [11]. In addition, the PhCs content also contributed to methanol diffusion in the membrane structure. The characteristic structure of PhCs was performed to block the methanol molecules [10]. However, the agglomeration did affect the resulting methanol permeability value. Excessive MWCNT/MMT filler could create aggregates in the membrane surface and tend to increase the methanol permeability [23]. This phenomenon is in agreement with SEM and AFM images.

3.7. Membrane selectivity

Selectivity is a significant parameter that showed the total performance of the composite membrane. Selectivity is determined by the ratio of conductivity and methanol permeability value. It is desired to have high conductivity and low methanol permeability [10-12]. The high selectivity shows a better performance of the membrane [36]. It is notable to decide the ideal loading of filler and additive to expand the role of new composite membranes in DMFC. It can be clearly shown in Table 2 that the membrane selectivity of Cs/PhCs/MWCNT/MMT-1 and Cs/PhCs/MWCNT/MMT-2 is higher than the commercial Nafion which indicates both the as-fabricated membranes are suitable for DMFC application. Cs/PhCs/MWCNT/MMT-1 can achieve the best membrane selectivity at 5.13×10^5 S.s.cm^{-3}. Furthermore, 7.5 wt.% loading of MWCNT and 2.5 wt.% loading of PhCs were considered as the best loading in the Cs matrix compared to the other as-fabricated membranes.

3.8. IEC and water uptake

The IEC value reflects the proton transfer with the Grotthus mechanism. Polymeric membrane incorporated with 7.5 wt.% loading of MWCNT/MMT filler had the highest IEC value compared to the pristine polymeric membrane. Moreover, the continuous increment of the loading of MWCNT/MMT filler tends to decrease the IEC value. Optimized loading of MWCNT/MMT filler should be added to the polymer matrix to achieve a high IEC value [28, 29]. The higher IEC value is more favorable than the lower IEC which indicates the hydrophilic groups take an important role to transfer the proton in the membrane structure [2]. According to Purwanto et al. [11], the improvement of IEC value was based on an excellent interaction of Cs/PhCs matrix and filler, especially MMT that lead to the enrichment of hydrophilic groups of the composite membrane. In addition, water uptake also gives a contribution to the proton transfer of membranes. The water uptake value typically indicates the vehicle or diffusion mechanism [2]. The highest water uptake is also attained by a composite membrane with 7.5 wt.% loading of filler in which the water uptake can reach up to 39.21%. Excessive loading of filler into the polymer matrix could decrease the water uptake value. Agglomeration of MWCNT/MMT filler in the composite could disrupt the membrane diffusion's channel of water [19]. The optimum loading of filler that can be achieved by a membrane was 7.5 wt.%. This phenomenon reveals that the composite membrane has both Grotthus and Vehicle mechanisms in the membrane structure to transport the proton. The IEC and water uptake of membranes are listed in Table 3.

3.9. DMFC performance test

DMFC performance evaluation is an important investigation that shows the response of the chemical structures of the membrane and proves the proton conductivity values. The power density value can be used to evaluate the performance of the membrane prior to implementing it in DMFC applications [13]. Figure 8 shows the DMFC performance of the composite membranes. The membranes with MWCNT/MMT loading exhibit a higher power density than PhCs loading. The CS/PhCs/MWCNT/MMT-1 membrane has the highest power density at 23.60 mW cm^{-2} compared to other membranes. The significant improvement of power density value is due to the improvement of proton conductivity value [29]. Moreover, the incorporation of filler contributes to an improvement in power density indirectly by increasing the membrane conductivity [37]. The presence of the MMT and MWCNT which contain hydroxyl groups and excellent conductivity could support the proton transfer in the membrane's structure [22,38]. The Cs/PhCs supported by MWCNT/MMT is a promising membrane for DMFC application. As expected, the Cs/PhCs/MWCNT/MMT membranes have better power density than the commercial Nafion which blended with Pd-SiO_2 and PBI-ZP. In the same condition, the blended Nafion membranes showed a low power density at 10.20 and 9.88 mW cm^{-2}, respectively [37]. The comparison of the power density of the composite membranes is shown in Table 4.

3.9. Morphological characteristics of composite membranes

The morphological characteristics of Cs/PhCs and Cs/PhCs/MWCNT/MMT membranes were observed using SEM. The cross-sectional SEM images are shown in Figure 9. It can be seen that the as-fabricated membranes show a smooth dense structure morphology. According to Muthumeenal et al. [10], the PhCs molecule facilitates sponge-like morphology which can absorb a large number of water molecules and it is desired to provide a proton transfer pathway. The similar morphology also showed in Figure 9(a) and (e) in which the sponge-like structure dominates the Cs/PhCs membrane structure. Furthermore, the Cs/PhCs membrane shows no agglomeration. This proved the phthalic molecules are well-dispersed into the Cs matrix, and the presence of carbonyl and hydroxyl group in PhCs have improved the interaction with other hydroxyl and amine groups in [39]. Modification of MMT with MWCNT has caused MWCNT/MMT filler to have more hydrophilic groups such as hydroxyl groups while SiO_2 from MMT makes it easier to interact with the hydroxyl and amine groups in Cs by forming hydrogen bonding [40]. Figure 9(b) and (f) show Cs/PhCs/MWCNT/MMT-1 membrane has less MMT agglomerated particles and no pinholes are formed in the membrane's structure. The absence of pinholes is favored for the DMFC application which could reduce the methanol permeability [34]. Figure 9(c) and (g) demonstrate the Cs/PhCs/MWCNT/MMT-2 membrane with the presence of agglomerates but without pinholes. This could be due to excessive loading of MWCNT/MMT filler that is not fully dispersed into the matrix and MMT is one of the aluminosilicate materials with high atomic numbers (Si and Al) [41]. The high atomic number of Si and Al tend to agglomerate easily in the polymer matrix and are visible in the SEM analysis. Additionally, the agglomeration which emerged in Cs/PhCs/MWCNT/MMT-2 membrane could disrupt the proton transfer pathway and diminish the proton conductivity [11]. These studies are in agreement with the physicochemical features of the membranes.

Table 2
Physicochemical properties of membranes.

Membrane	Methanol permeability (cm^2.s^{-1})	Proton conductivity (mS.cm^{-1})	Selectivity (S.s.cm^{-3})
Cs/PhCs	1.51×10^{-4}	2.44	0.16×10^2
Cs/PhCs/MWCNT/MMT-1	7.71×10^{-9}	3.95	5.13×10^5
Cs/PhCs/MWCNT/MMT-2	2.51×10^{-8}	0.39	1.56×10^4
Nafion 117[a]	2.50×10^{-6}	31.60	1.26×10^4

[a] Nafion 117 performances adapted from [11]

Table 3
IEC and water uptake value.

Membrane	IEC (meq.g^{-1})	Water uptake (%)
Cs/PhCs	0.771	34.75
Cs/PhCs/MWCNT/MMT-1	0.856	39.21
Cs/PhCs/MWCNT/MMT-2	0.743	37.45

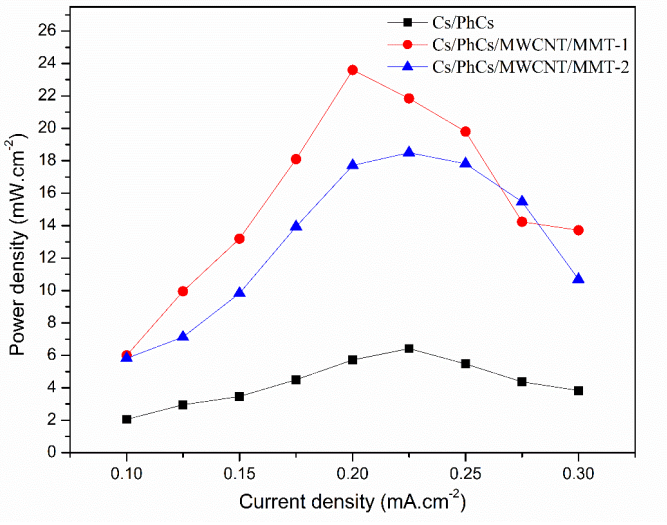

Fig. 8 DMFC performance of each membrane.

3.10. Topographical characteristics of composite membranes

Atomic force microscopy is used to determine the topography of membranes [42]. The phase and surface topography of the Cs/PhCs and Cs/PhCs/MWCNT/MMT composite membranes were observed by the AFM technique to determine the impacts of MWCNT/MMT filler reinforcing Cs matrix. Figure 10 shows the phase images of the Cs/PhCs membrane and composite membranes. The bright and dark areas on the membrane's surface represented hydrophilic and hydrophobic morphologies, respectively [10]. Figure 10(a) shows the Cs/PhCs membrane surface that demonstrates brighter areas. It could be due to the addition of the phthalate group into the Cs matrix which indirectly improved the hydrophilic groups in the membrane. Furthermore, the brighter areas also explained that PhCs could disperse into the Cs matrix. On the other hand, Figure 10(b) and (c) demonstrate that the Cs/PhCs/MWCNT/MMT-1 membrane showed uniformly brighter areas than Cs/PhCs/MWCNT/MMT-2 as a result of the excessive loading of the MWCNT/MMT filler. The Cs/PhCs/MWCNT/MMT-2 membrane only had several brighter domains on its surface which indicate the filler aggregates [29, 41].

The surface roughness of membranes is listed in Table 5. The highest surface roughness can be observed in Cs/PhCs/MWCNT/MMT-2 which had average roughness (Sa), root mean square roughness (Sq), and maximum height (Sz) of 93.1 nm, 116 nm, and 748 nm, respectively. It has higher surface roughness than the other as-fabricated membranes. The value of the roughness was attributed to the filler agglomeration. Moreover, the agglomeration could mainly disrupt the proton conductivity of the membrane [10]. The best AFM result is showed by Cs/PhCs/MWCNT/MMT-1 membrane which had moderate surface roughness for DMFC application.

Table 4
Maximum power density of composite membrane at room temperature operation.

Membrane	Methanol concentration (M)	Maximum power density ($mW.cm^{-2}$)	Reference
Cs/PhCs	5	6.42	This work
Cs/PhCs/MWCNT/MMT-1	5	23.60	This work
Cs/PhCs/MWCNT/MMT-2	5	18.50	This work
Pd-SiO_2/Nafion	2	10.20	[37]
Nafion-PBI-ZP	5	9.88	[37]

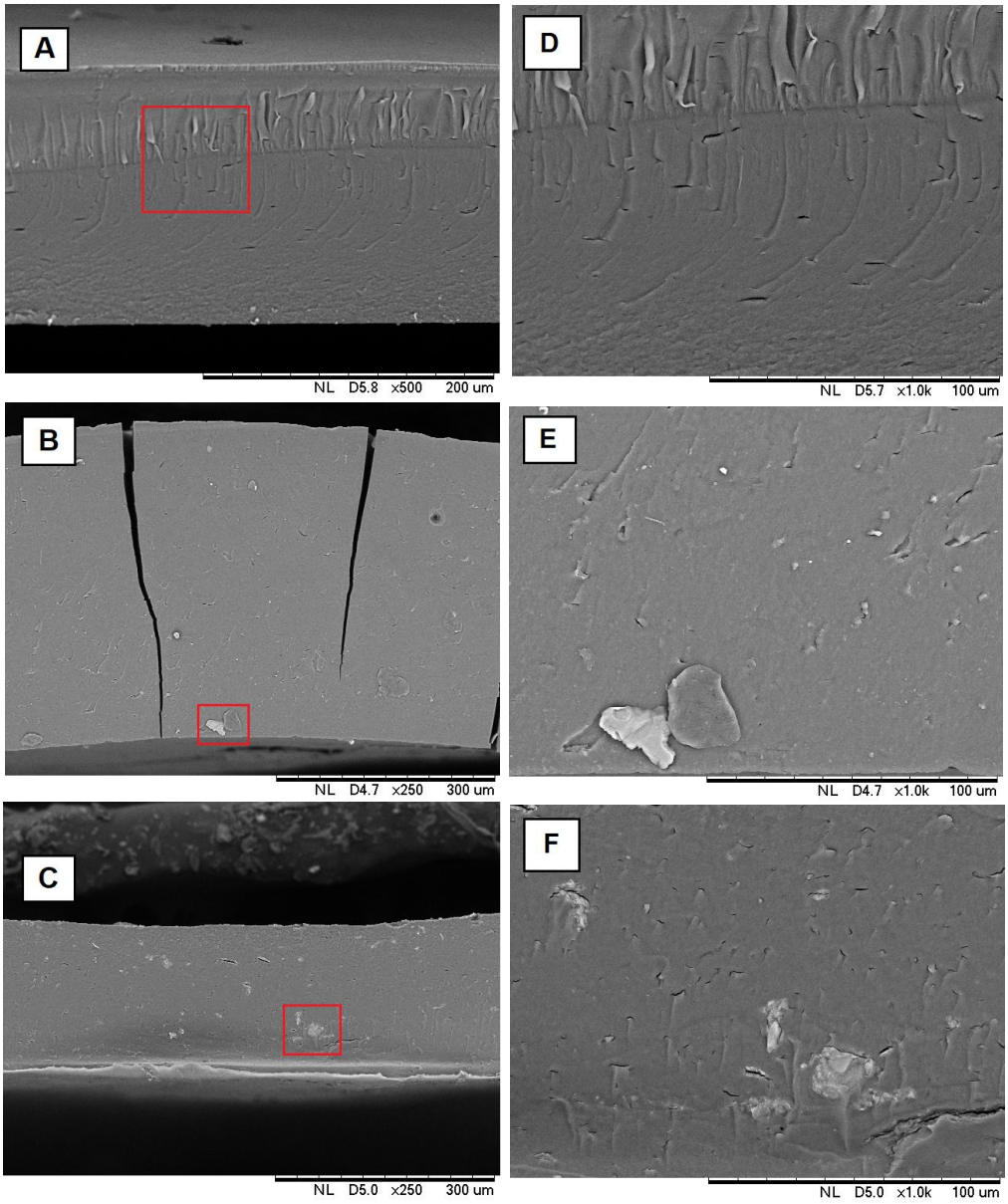

Fig. 9 Cross-sectional images of (a) Cs/PhCs at 500×, (b) Cs/PhCs/MWCNT/MMT-1, (c) Cs/PhCs/MWCNT/MMT-2 membranes at magnification 250×; (d), (e), and (f) membranes at magnification 1000×.

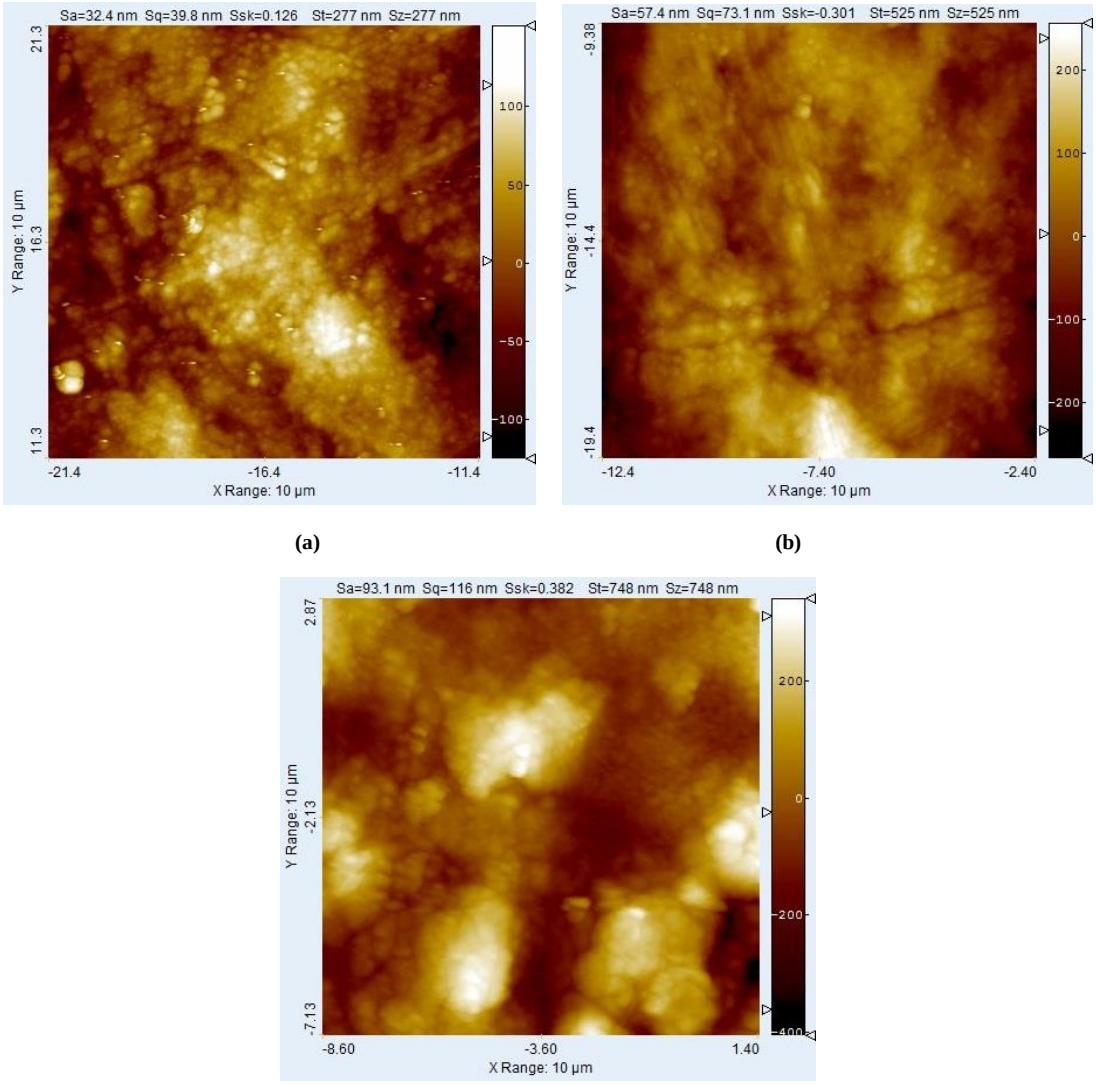

Fig. 10. Surface topography of (a) Cs/PhCs, (b) Cs/PhCs/MWCNT/MMT-1, and (c) Cs/PhCs/MWCNT/MMT-2 membranes.

Table 5
Surface roughness for each membrane.

Membrane	Sa (nm)	Sq (nm)	Sz (nm)
Cs/PhCs	32.4	39.8	277
Cs/PhCs/MWCNT/MMT-1	57.4	73.1	525
Cs/PhCs/MWCNT/MMT-2	93.1	116	748

Figure 11 shows the three-dimensional images of all membranes. The result revealed that Cs/PhCs/MWCNT/MMT-2 had more shark peaks than the Cs/PhCs and Cs/PhCs/MWCNT/MMT-1 membranes. Figure 11 supports the two dimensional AFM images that explained the addition of the MWCNT/MMT filler into the Cs matrix led to the increment of surface roughness. Therefore, there is a relation between the AFM peaks and surface roughness values. According to Chrzanowska et al. [43], the incorporation of MMT nanoparticle into the Cs biopolymer could significantly affect the surface roughness of the resulting composite membranes. The undispersed MMT also affects the topography and surface roughness of the resulting composite membranes. It can lead to an increase in the surface roughness of the resulting membranes [10]. From the AFM study, it can be decided that the Cs/PhCs/MWCNT/MMT-1 membrane is appropriate for DMFC application.

4. Conclusions

In this study, the newly composite membranes developed from the modified chitosan by PhCs with various loading of MWCNT/MMT filler were successfully fabricated by using the solvent evaporation method. FTIR, SEM, and AFM were performed to determine chemical interaction, morphology, and topography of the composite membranes. The findings show that there were new functional groups that were found in composite membranes such as Si-O-Si, Si-OH, and Si-O groups. These bands typically came from MWCNT/MMT and were confirmed that the filler has been successfully incorporated into the membrane matrix. SEM images of cross-sectional were conducted which revealed the addition of MWCNT/MMT filler has caused the changes in the membranes structure. The higher loading of MWCNT/MMT filler has caused agglomeration in the membrane's structure. According to the AFM images, the Cs/PhCs/MWCNT/MMT-1 membrane had moderate surface roughness which is suitable for the DMFC application. Furthermore, the morphology and topography studies are in agreement with the membrane's performances in which the Cs/PhCs/MWCNT/MMT-1 membrane had the best membrane selectivity of 5.13×10^{5} S.s.cm^{-3} and the DMFC performance was at 23.60 mW.cm^{-2}. It can be said that the Cs membrane consisted of 2.5 wt.% loading PhCs and 7.5 wt.% loading MWCNT/MMT filler can be an alternative polyelectrolyte membrane for the DMFC application.

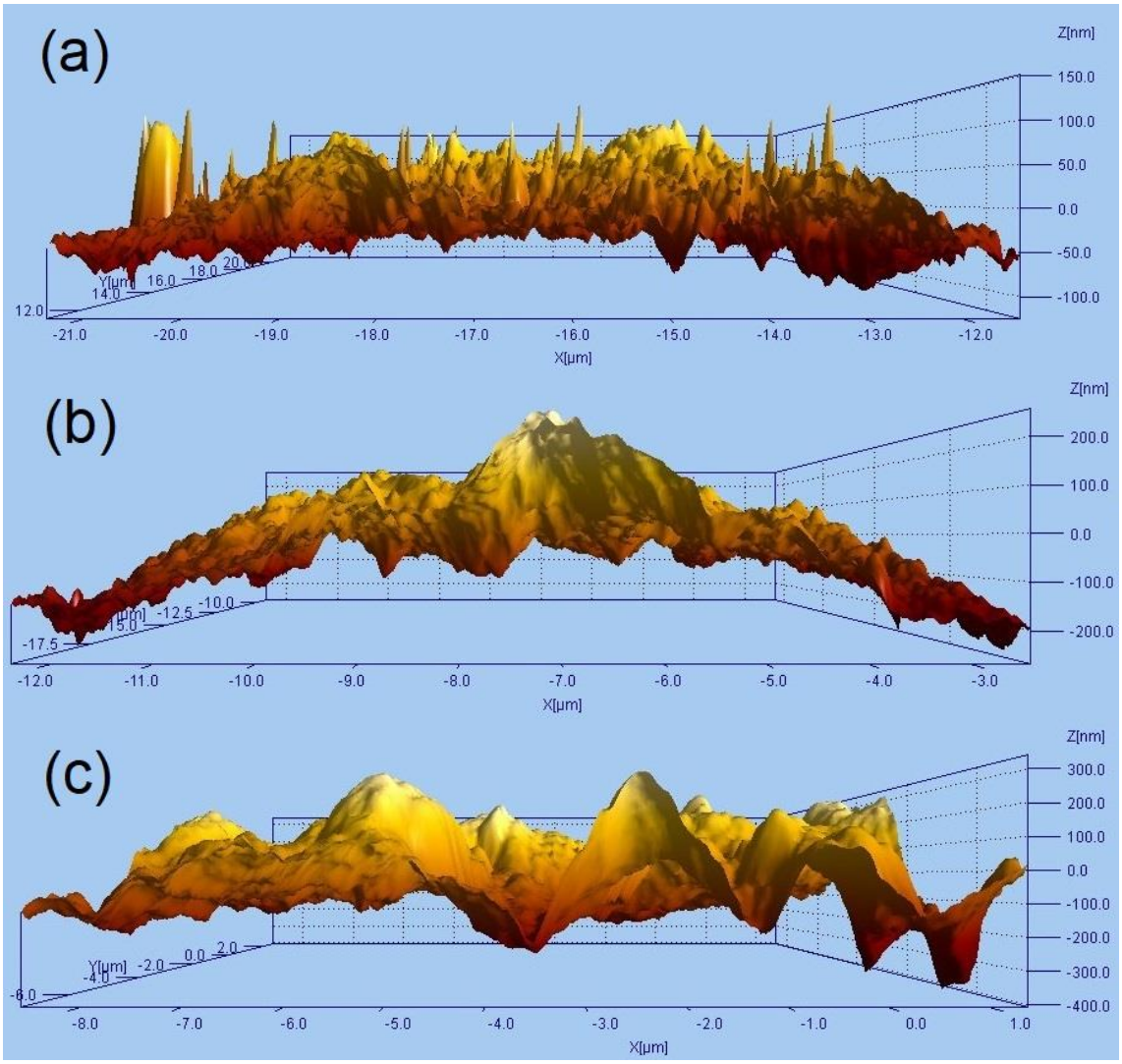

Fig. 11. Three dimensional topography of (a) Cs/PhCs, (b) Cs/PCs/MWCNT/MMT-1, and (c) Cs/PhCs/MWCNT/MMT-2 membranes.

Acknowledgments

This research was supported by the Material Chemistry and Energy laboratory, Department of Chemistry, Institut Teknologi Sepuluh Nopember. The authors also thank the Advanced Membrane Technology Research Centre (AMTEC), Universiti Teknologi Malaysia for associating the research and to be a joint research university partner.

References

[1] K. Pourzare, Y. Mansourpanah, S. Farhadi, Advanced nanocomposite membranes for fuel cell applications : a comprehensive review, Biofuel Res. J. 12 (2016) 496–513. DOI: 10.18331/BRJ2016.3.4.4.

[2] F.C. Teixeira, A.I. de Sá, A.P.S. Teixeira, C.M. Rangel, Nafion phosphonic acid composite membranes for proton exchange membranes fuel cells, Appl. Surf. Sci. 487 (2019) 889–97. DOI:10.1016/j.apsusc.2019.05.078.

[3] R. Stropnik, M. Sekavčnik, A.M. Ferriz, M. Mori, Reducing environmental impacts of the ups system based on PEM fuel cell with circular economy, Energy. 165 (2018) 824–35. DOI:10.1016/j.energy.2018.09.201.

[4] J. Wang, Barriers of scaling-up fuel cells: Cost, durability and reliability, Energy. 80 (2015) 509–21. DOI:10.1016/j.energy.2014.12.007.

[5] Z.P. Cano, D. Banham, S. Ye, A. Hintennach, J. Lu, M. Fowler, Batteries and fuel cells for emerging electric vehicle markets, Nat. Energy. 3 (2018) 279–89. DOI:10.1038/s41560-018-0108-1.

[6] A. Kraytsberg, and Y. Ein-Eli, Review of advanced materials for proton exchange membrane fuel cells, Energy and Fuels. 28 (2014) 7303–30. DOI: 10.1021/ef501977k.

[7] A.R. Kim, C.J. Park, M. Vinothkannan, D.J. Yoo, Sulfonated poly ether sulfone/heteropoly acid composite membranes as electrolytes for the improved power generation of proton exchange membrane fuel cells, Compos. B. Eng. 155 (2018) 272–81. DOI:10.1016/j.compositesb.2018.08.016.

[8] C. Yin, J. Li, Y. Zhou, H. Zhang, P. Fang, C. He, Enhancement in Proton Conductivity and Thermal Stability in Nafion Membranes Induced by Incorporation of Sulfonated Carbon Nanotubes, ACS Appl. Mater. Interfaces. 10 (2018) 14026–35. DOI: 10.1021/acsami.8b01513.

[9] A. Kusoglu, A.Z. Weber, New Insights into Perfluorinated Sulfonic-Acid Ionomers, Chem. Rev. 117 (2017) 987–1104. DOI: 10.1021/acs.chemrev.6b00159.

[10] A. Muthumeenal, S. Neelakandan, P. Kanagaraj, A. Nagendran, Synthesis and properties of novel proton exchange membranes based on sulfonated polyethersulfone and N-phthaloyl chitosan blends for DMFC applications, Renew. Energ. 86 (2016) 922–9. DOI:10.1016/j.renene.2015.09.018.

[11] M. Purwanto, L. Atmaja, M.A. Mohamed, M.T. Salleh, J. Jaafar, A.F. Ismail, Biopolymer-based electrolyte membranes from chitosan incorporated with montmorillonite-crosslinked GPTMS for direct methanol fuel cells, RSC Adv. 6 (2016) 2314–22. DOI:10.1039/C5RA22420A.

[12] V. Vijayakumar, and D. Khastgir, Hybrid composite membranes of chitosan/sulfonated polyaniline/silica as polymer electrolyte membrane for fuel cells, Carbohydr. Polym. 179 (2018) 152–63. DOI:10.1016/j.carbpol.2017.09.083.

[13] N. Awang, A.F. Ismail, J. Jaafar, T. Matsuura, H. Junoh, M.H.D. Othman, Functionalization of polymeric materials as a high performance membrane for direct methanol fuel cell: A review, React. Funct. Polym. 86 (2015) 248–58. DOI:10.1016/j.reactfunctpolym.2014.09.019.

[14] K. Hari Gopi, V.M. Dhavale, S.D. Bhat, Development of polyvinyl alcohol/chitosan blend anion exchange membrane with mono and di quaternizing agents for application in alkaline polymer electrolyte fuel cells, Mater. Sci. Energy. Technol. 2 (2019) 194–202. DOI:10.1016/j.mset.2019.01.010.

[15] C.Z. Bueno, A.M. Moraes, H.C. De Sousa, M.E.M Braga, Effects of supercritical carbon dioxide processing on the properties of chitosan-alginate membranes, J. Supercrit. Fluids. 112 (2016) 128–35. DOI: 10.1016/j.supflu.2015.10.001.

[16] A.K.S. Anu Karthi, and L. Cindrella, Self-humidifying novel chitosan-geopolymer hybrid membrane for fuel cell applications, Carbohydr. Polym. 223 (2019) 115073. DOI:10.1016/j.carbpol.2019.115073.

[17] P. Chen, L. Hao, W. Wu, Y. Li, J. Wang, Polymer-inorganic hybrid proton conductive membranes: Effect of the interfacial transfer pathways, Electrochim. Acta. 212 (2016) 426–39. DOI:10.1016/j.electacta.2016.07.001.

[18] Y. Zhao, H. Yang, H. Wu, Z. Jiang, Enhanced proton conductivity of hybrid membranes by incorporating phosphorylated hollow mesoporous silica submicrospheres, J. Membr. Sci. 469 (2014) 418–27. DOI:10.1016/j.memsci.2014.07.004.

[19] Y. Yin, T. Xu, X. Shen, H. Wu, Z. Jiang, Fabrication of chitosan/zwitterion functionalized titania-silica hybrid membranes with improved proton conductivity, J. Membr. Sci. 469 (2014) 355–63. DOI:10.1016/j.memsci.2014.07.003.

[20] H. Sadegh, K. Zare, B. Maazinejad, R. Shahryari-Ghoshekandi, I. Tyagi, S. Agarwal, Synthesis of MWCNT-COOH-Cysteamine composite and its application for dye removal, J. Mol. Liq. 215 (2016) 221–8. DOI:10.1016/j.molliq.2015.12.042.

[21] W. Wang, B. Shan, L. Zhu, C. Xie, C. Liu, F. Cui, Anatase titania coated CNTs and sodium lignin sulfonate doped chitosan proton exchange membrane for DMFC application, Carbohydr. Polym. 187 (2018) 35–42. DOI:10.1016/j.carbpol.2018.01.078.

[22] B. Peng, C. Takai, H. Razavi-khosroshahi, M. Fuji, Effect of silane modification on CNTs/silica composites fabricated by a non-firing process to enhance interfacial property and dispersibility, Adv. Powder Technol. 29 (2018) 2091–6. DOI:10.1016/j.apt.2018.05.017.

[23] D. Manikandan, R.V. Mangalaraja, R.E. Avila, R. Siddheswaran, S. Ananthakumar, Carbon nanotubes rooted montmorillonite (CNT-MM) reinforced nanocomposite membrane for PEM fuel cells, Mater. Sci. Eng. B Solid-State Mater. Adv. Technol. 177 (2012) 614–8. DOI:10.1016/j.mseb.2012.02.027.

[24] H. Liu, C. Gong, J. Wang, X. Liu, H. Liu, F. Cheng, Chitosan/silica coated carbon nanotubes composite proton exchange membranes for fuel cell applications, Carbohydr. Polym. 136 (2016) 1379–85. DOI:10.1016/j.carbpol.2015.09.085.

[25] S. Mallakpour, and S. Soltanian, Surface functionalization of carbon nanotubes: Fabrication and applications, RSC Adv. 6 (2016) 109916–35. DOI: 10.1039/C6RA24522F.

[26] I. Younes, and M. Rinaudo, Chitin and chitosan preparation from marine sources. Structure, properties and applications, Mar. Drugs. 13 (2015) 1133–74. DOI: 10.3390/md13031133.

[27] T. Si Trung, and H.N.D. Bao, Physicochemical Properties and Antioxidant Activity of Chitin and Chitosan Prepared from Pacific White Shrimp Waste, Int. J. Carbohydr. Chem. (2015) 1–6. DOI: 10.1155/2015/706259.

[28] S.N.F. Yusuf, A.D. Azzahari, R. Yahya, S.R. Majid, M,A, Careem, A.K. Arof, From crab shell to solar cell: A gel polymer electrolyte based on N-phthaloylchitosan and its application in dye-sensitized solar cells, RSC Adv. 6 (2016) 27714–24. DOI: 10.1039/C6RA04188D.

[29] Y. Ou, W.C. Tsen, C. Gong, J. Wang, H. Liu, G. Zheng, Chitosan-based composite membranes containing chitosan-coated carbon nanotubes for polymer electrolyte membranes, Polym. Adv. Technol. 29 (2018) 612–22. DOI: 10.1002/pat.4171.

[30] R. Zhang, C. Chen, J. Li, X. Wang, Preparation of montmorillonite@carbon composite and its application for U(VI) removal from aqueous solution, Appl. Surf. Sci. 349 (2015) 129–37. DOI:10.1016/j.apsusc.2015.04.222.

[31] H. Lade, V. Kumar, G. Arthanareeswaran, A.F. Ismail, Sulfonated poly(arylene ether sulfone) nanocomposite electrolyte membrane for fuel cell applications: A review, Int. J. Hydrog. Energy. 42 (2017) 1063–74. DOI:10.1016/j.ijhydene.2016.10.038.

[32] M.H. Gouda, W. Gouveia, M.L. Afonso, B. Šljukić, N.A. El Essawy, A.B.A.A. Nassr, Poly(vinyl alcohol)-based crosslinked ternary polymer blend doped with sulfonated graphene oxide as a sustainable composite membrane for direct borohydride fuel cells, J. Power Sources. 432 (2019) 92–101. DOI: 10.1016/j.jpowsour.2019.05.078.

[33] Y. Yang, T.H. Le, F. Kang, M. Inagaki, Polymer blend techniques for designing carbon materials, Carbon. 111 (2017) 546–68. DOI:10.1016/j.carbon.2016.10.047.

[34] H. Lee, J. Han, K. Kim, J. Kim, E. Kim, H. Shin, Highly sulfonated polymer-grafted graphene oxide composite membranes for proton exchange membrane fuel cells, J. Ind. Eng. Chem. 74 (2019) 223–32. DOI:10.1016/j.jiec.2019.03.012.

[35] Q. Zhao, Y. Wei, C. Ni, L. Wang, B. Liu, J. Liu, Effect of aminated nanocrystal cellulose on proton conductivity and dimensional stability of proton exchange membranes, Appl. Surf. Sci. 466 (2019) 691–702. DOI:10.1016/j.apsusc.2018.10.063.

[36] H. Nagar, N. Sahu, V.V. Basava Rao, S. Sridhar, Surface modification of sulfonated polyethersulfone membrane with polyaniline nanoparticles for application in direct methanol fuel cell, Renew. Energ. 146 (2020) 1262–77. DOI:10.1016/j.renene.2019.06.175.

[37] F.A. Zakil, S.K. Kamarudin, S. Basri, Modified Nafion membranes for direct alcohol fuel cells: An overview, Renew. Sust. Energ. Rev. 65 (2016) 841–52. DOI: 10.1016/j.rser.2016.07.040.

[38] K. Charradi, Z. Ahmed, P. Aranda, R. Chtourou, Silica/montmorillonite nanoarchitectures and layered double hydroxide-SPEEK based composite membranes for fuel cells applications, Appl. Clay. Sci. 174 (2019) 77–85. DOI:10.1016/j.clay.2019.03.027.

[39] N. Shaari, S.K. Kamarudin, S. Basri, L.K. Shyuan, M.S. Masdar, D. Nordin, Enhanced Proton Conductivity and Methanol Permeability Reduction via Sodium Alginate Electrolyte-Sulfonated Graphene Oxide Bio-membrane, Nanoscale Res. Lett. 13 (2018). DOI:10.1186/s11671-081-2493-6.

[40] V.G.L. Souza, J.R.A. Pires, E.T. Vieira, I.M. Coelhoso, M.P. Duarte, A.L. Fernando, Activity of chitosan-montmorillonite bionanocomposites incorporated with rosemary essential oil: From in vitro assays to application in fresh poultry meat, Food Hydrocoll. 89 (2019) 241–52. DOI:10.1016/j.foodhyd.2018.10.049.

[41] M. Gierszewska, E. Jakubowska, E. Olewnik-Kruszkowska, Effect of chemical crosslinking on properties of chitosan-montmorillonite composites, Polym. Test. 77 (2019) 1058-72. DOI:10.1016/j.polymertesting.2019.04.019.

[42] V. Vijayalekshmi, and D. Khastgir, Fabrication and comprehensive investigation of physicochemical and electrochemical properties of chitosan-silica supported silicotungstic acid nanocomposite membranes for fuel cell applications, Energy. 142 (2018) 313–30. DOI:10.1016/j.energy.2017.10.019.

[43] E. Chrzanowska, M. Gierszewska, J. Kujawa, A. Raszkowska-Kaczor, W. Kujawski, Development and characterization of polyamide-supported chitosan nanocomposite membranes for hydrophilic pervaporation, Polymers. 10 (2018) 1–21. DOI: 10.3390/polym10080868.